

Finite-size effects at the hadron-quark transition and heavy hybrid stars

Nobutoshi Yasutake,^{1,*} Rafał Lastowiecki,^{2,†} Sanjin Benić,^{3,‡} David Blaschke,^{2,4,§} Toshiaki Maruyama,^{5,¶} and Toshitaka Tatsumi^{6,**}

¹*Department of Physics, Chiba Institute of Technology,
2-1-1 Shibazono, Narashino, Chiba 275-0023, Japan*

²*Institute for Theoretical Physics, University of Wrocław, Max Born pl. 9, 50-204 Wrocław, Poland*

³*Physics Department, Faculty of Science, University of Zagreb, Zagreb 10000, Croatia*

⁴*Bogoliubov Laboratory for Theoretical Physics, JINR Dubna, 141980 Dubna, Russia*

⁵*Advanced Science Research Center, Japan Atomic Energy Agency, Tokai, Ibaraki 319-1195, Japan*

⁶*Department of Physics, Kyoto University, Kyoto 606-8502, Japan*

(Dated: May 24, 2022)

We study the role of finite-size effects at the hadron-quark phase transition in a new hybrid equation of state constructed from an ab-initio Brückner-Hartree-Fock equation of state with the realistic Bonn-B potential for the hadronic phase and a covariant non-local Nambu–Jona-Lasinio model for the quark phase. We construct static hybrid star sequences and find that our model can support stable hybrid stars with an onset of quark matter below $2 M_\odot$ and a maximum mass above $2.17 M_\odot$ in agreement with recent observations. If the finite-size effects are taken into account the core is composed of pure quark matter. Provided that the quark vector channel interaction is small, and the finite size effects are taken into account, quark matter appears at densities 2-3 times the nuclear saturation density. In that case the proton fraction in the hadronic phase remains below the value required by the onset of the direct URCA process, so that the early onset of quark matter shall affect on the rapid cooling of the star.

PACS numbers: 26.60.+c, 97.60.Jd, 21.65.+f, 12.39.-x

I. INTRODUCTION

The equation of state (EoS) is the central quantity for the study of compact stars. Since modern lattice QCD simulations are not applicable at large baryon densities and low temperatures $T \simeq 0$, there is a large uncertainty in theoretical descriptions of the behavior of matter at extreme densities. The understanding may be improved by studying astrophysical phenomena; namely, we may use the known astrophysical constraints from observations of compact stars in order to provide constraints on the EoS. Recently, the idea has been pursued to use a Bayesian analysis (BA) for “inversion” of the Tolman–Oppenheimer–Volkoff equations, i.e. to extract a probability measure for models of the cold EoS in the pressure–energy density plane from observational data related to masses and radii of compact stars. While first analyses of this type have favored burst sources with rather uncertain and model dependent statements about radii [1, 2], a very recent BA uses a set of stronger and statistically independent observations, testing also the possibility of a first order phase transition at supersaturation densities [3].

At this point the strongest restriction to the EoS is provided by the recent measurement of the high mass of

$\sim 2 M_\odot$ from observations of the pulsars PSR J1614-2230 by Demorest et. al. [4] and PSR J0348+0432 by Antoniadis et. al. [5]. The recent BA [3] makes use of this constraint together with a new mass-radius constraint from the precise timing analysis of the nearest known millisecond pulsar PSR J0437-4715 [6] and the constraint on the gravitational binding for the neutron star B in the binary system J0737-3039(B) [7], see also [8], at the precisely measured gravitational mass of $1.249 \pm 0.001 M_\odot$.

There are many studies relating astrophysical phenomena involving compact stars and the properties of matter at extreme densities, eventually including the possibility of a quark deconfinement transition. These concern, e. g., the cooling of compact stars [9–12], gravitational wave emission [13–15], neutrino emission [16–18], eigenfrequencies [19], and the energy release during the collapse of neutron stars to quark stars [20–22].

The study of the baryon-baryon (BB) interaction in lattice QCD simulations recently became a hot topic [23, 24]. Experiments like JPARC will also provide valuable information on the BB interaction. In the near future the EoS in the hadronic phase may be determined by incorporating this information on the BB interaction in the Brückner-Hartree-Fock (BHF) theory [25], the variational approach [26, 27], or the Dirac-Brückner-Hartree-Fock (DBHF) theory [28, 29]. In this paper we adopt the BHF theory for hadronic matter.

Out of a several of possible models for quark matter we use the two flavor covariant non-local Nambu–Jona-Lasinio (nlNJL) model [30, 31] with vector interactions [32]. The advantage over the usual local version of the NJL model is due to the introduction of the addi-

* nobutoshi.yasutake@it-chiba.ac.jp

† lastowiecki@ift.uni.wroc.pl

‡ sanjinb@phy.hr

§ blaschke@ift.uni.wroc.pl

¶ maruyama.toshiaki@jaea.go.jp

** tatsumi@ruby.scphys.kyoto-u.ac.jp

tional gradient self-energy channel and due to the explicit momentum dependence of all the dressing functions of the quark propagator. Both of these improvements are well founded on lattice QCD data [33, 34] and Dyson-Schwinger equation studies [35–37], and make the non-local NJL model a well-calibrated, effective low-energy QCD approach to the thermodynamics of quark matter.

The main purpose of this work is to examine the features and the astrophysical consequences of the mixed phase between the pure quark and hadron matter phases by considering *finite-size effects*. Taking into account the surface tension and the charge screening we find the non-uniform, so-called “pasta” structures at the hadron-quark interface. In this work we investigate more in detail the occurrence of pasta structures for the values of the surface tension $\sigma = 10 \text{ MeV fm}^{-2}$ and 40 MeV fm^{-2} . For weak surface tension the EoS of the mixed phase becomes similar to the one of a bulk Gibbs construction, while for strong surface tension it approaches the result of a Maxwell construction [38–41], in which the maximum masses with the phase transition are around $1.5M_\odot$ and a simple bag model was used for modeling the quark phase. This model gives a quite simple description of quark matter, and it should be replaced by a more sophisticated one to study more realistically the quark-hadron phase transition. This is the aim of the present work.

We construct the hybrid EoS and the corresponding hybrid star sequences. For the calculation of the quark matter EoS we use the following values for the ratio of the vector and the scalar channel couplings $\eta_V = G_V/G_S = 0.10$ and $\eta_V = 0.20$. Stable hybrid stars respecting the $2 M_\odot$ constraint are found in the case of $\eta_V = 0.10$. The bulk Gibbs construction for this case supports only a mixed phase in the core. However, taking into account finite-size effects the cores of massive hybrid stars are composed of pure quark matter. For $\eta_V = 0.20$ the $2M_\odot$ stars are mainly composed of hadron matter. With the appearance of quark matter at higher densities the star becomes unstable. For $\eta_V = 0.10$ quark matter appears at low densities causing a reduction of the proton fraction at the onset of the mixed phase below the threshold value of $1/9$ for the onset of the direct URCA (dURCA) process in the $n - p - e$ phase, while for $\eta_V = 0.20$ the proton fraction exceeds this value.

This paper is organized as follows. In Sec. II, we outline our framework for obtaining the hybrid EoS with pasta phase. Sec. III contains numerical results for the EoS with the different quark-hadron mixed phase constructions including the pasta phase as well as for the corresponding compact star sequences. Sec. IV is devoted to the conclusion and a discussion of some astrophysical implications of our results.

II. EQUATION OF STATE

A. Equation of state for quark phase

—non-local NJL model

The current theoretical description of quark matter includes many uncertainties, seriously limiting the predictability of the EoS at high baryon density. We resort here to a field theoretical model for the quark matter EoS and apply constraints on parameters from available experimental information and lattice QCD data. We will use the $N_f = 2$ covariant non-local Nambu–Jona–Lasinio (nlNJL) model [30, 31]. For some of the previous works on the cold, dense EoS in this class of models see Ref. [42] for superconductivity, [43] for application to $2 + 1$ flavors and [32] where a crossover transition was discussed at $T = 0$.

At $T = 0$ the Euclidean action is given as [30, 31]

$$S_E = \int d^4x [\bar{q}(-i\partial_\mu\gamma_\mu + m)q - i\mu\bar{q}\gamma_4q - \frac{G_S}{2} \{j_a^S(x)j_a^S(x) + j_{\mathbf{p}}(x)j_{\mathbf{p}}(x) + j_{p_4}(x)j_{p_4}(x)\} + \frac{G_V}{2} j_\mu^V(x)j_\mu^V(x)], \quad (1)$$

with currents

$$j_a^S(x) = \int d^4z g(z)\bar{q}\left(x + \frac{z}{2}\right)\Gamma_a q\left(x - \frac{z}{2}\right), \quad (2)$$

$$j_{\mathbf{p}}(x) = \int d^4z f(z)\bar{q}\left(x + \frac{z}{2}\right)\frac{i\overleftrightarrow{\nabla} \cdot \boldsymbol{\gamma}}{2\kappa_{\mathbf{p}}}q\left(x - \frac{z}{2}\right), \quad (3)$$

$$j_{p_4}(x) = \int d^4z f(z)\bar{q}\left(x + \frac{z}{2}\right)\frac{i\overleftrightarrow{\partial}_4\gamma_4}{2\kappa_{p_4}}q\left(x - \frac{z}{2}\right), \quad (4)$$

where $\Gamma_a = (1, i\gamma_5\boldsymbol{\tau})$, $\boldsymbol{\tau}$ are Pauli matrices and m, μ are the current quark mass set as $m = 2.37 \text{ MeV}$ for u, d -quarks, and the quark chemical potential. The vector current

$$j_\mu^V(x) = \bar{q}(x)\gamma_\mu q(x), \quad (5)$$

is kept in a local form. By different weights $\kappa_{\mathbf{p}} \neq \kappa_{p_4}$ of the derivative currents $j_{\mathbf{p}}$ and j_{p_4} we are anticipating medium induced Lorentz symmetry breaking. The relation between the parameters $\kappa_{\mathbf{p}}^2/\kappa_{p_4}^2 = 3$ restores Lorentz symmetry in the vacuum.

Within the mean-field approximation the regularized thermodynamic potential takes the following form

$$\Omega = \Omega_{\text{cond}} + \Omega_{\text{kin}}^{\text{reg}} + \Omega_{\text{free}}^{\text{reg}}, \quad (6)$$

$$\Omega_{\text{cond}} = \frac{1}{2G_S} (\sigma_B^2 + \kappa_{\mathbf{p}}^2\sigma_A^2 + \kappa_{p_4}^2\sigma_C^2) - \frac{\omega^2}{2\eta_V G_S}, \quad (7)$$

$$\Omega_{\text{kin}}^{\text{reg}} = -N_f N_c \int \frac{d^4p}{(2\pi)^4} \text{tr}_D \log \left[\frac{S^{-1}(\tilde{p})}{S_0^{-1}(\tilde{p})} \right], \quad (8)$$

and

$$\Omega_{\text{free}}^{\text{reg}} = -\frac{N_f N_c}{24\pi^2} \left\{ 2\tilde{\mu}^3 \tilde{p}_F - 5m^2 \tilde{\mu} \tilde{p}_F + 3m^4 \log \left(\frac{\tilde{p}_F + \tilde{\mu}}{m} \right) \right\},$$

$$\tilde{p}_F = \sqrt{\tilde{\mu}^2 - m^2}. \quad (9)$$

Here

$$S^{-1}(\tilde{p}) = -(\boldsymbol{\gamma} \cdot \mathbf{p}) A(\tilde{p}^2) - \gamma_4 \tilde{p}_4 C(\tilde{p}^2) + B(\tilde{p}^2), \quad (10)$$

is the dressed quark propagator with the scalar and vector dressings

$$\begin{aligned} A(p^2) &= 1 + \sigma_A f(p^2), \\ B(p^2) &= m + \sigma_B g(p^2), \\ C(p^2) &= 1 + \sigma_C f(p^2) \end{aligned} \quad (11)$$

and $S_0(p)$ is the free quark propagator. We have introduced a shorthand $\tilde{p} = (\mathbf{p}, \tilde{p}_4)$ where $\tilde{p}_4 = p_4 - i\tilde{\mu}$ and $\tilde{\mu} = \mu - \omega$.

The usage of the non-local approach has the important advantage of fitting the form-factors $g(p^2)$ and $f(p^2)$ to lattice data for dynamical scalar $B(p^2)$ and vector dressing $A(p^2)$ [33, 34, 44]. Let us also mention that the strong infrared running of the QCD correlation functions is a core feature of the Dyson-Schwinger approaches [36, 37]. In this work we adopt the parametrization from [44].

The model is solved by finding the extremum of Eq. (6) with respect to the mean-fields $X = \sigma_A, \sigma_B, \sigma_C, \omega$

$$\frac{\partial \Omega}{\partial X} = 0. \quad (12)$$

The EoS is obtained from evaluating the thermodynamic potential at the extremum

$$p = -\Omega + \Omega_0, \quad (13)$$

where the constant Ω_0 ensures zero pressure in the vacuum.

B. Equation of state for hadron phase —Brückner-Hartree-Fock theory

Our theoretical framework for the hadron phase of matter is the nonrelativistic Brueckner-Hartree-Fock approach [25] based on the microscopic nucleon-nucleon (NN) potentials. The Brückner-Hartree-Fock calculation is a reliable and well-controlled theoretical approach for the study of dense baryonic matter. The detailed procedure can be found in Refs. [45–47]. In this paper, we do not consider hyperon degrees of freedom, since they are superseded by the existence of quarks as we suggested [41].

For the NN interaction we adopt the so-called Bonn-B (BOB) potential [48]. We also use semi-phenomenological Urbana UIX nucleonic three body

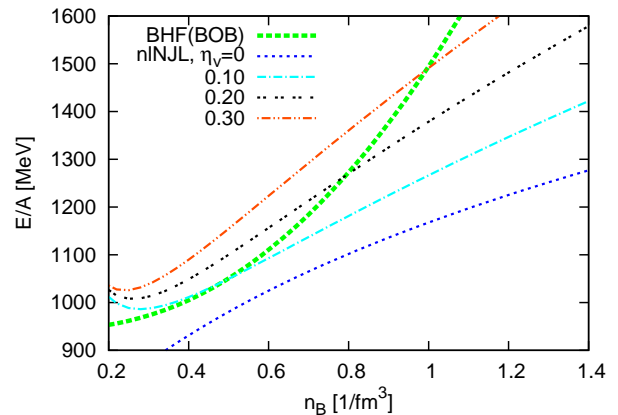


FIG. 1. (Color online) Energy per baryon E/A in comparison with pure hadron(thick curve) and quark phases(thin curves) for different values of the vector coupling η_V as indicated on the plot.

forces (TBF) [49]. The nucleon mass is given as $m_n = m_p = 939$ MeV.

On Fig. 1 we show the resulting EoS of the pure hadron (thick curve with the caption “BHF(BOB)”) and the pure quark phase (thin curves with the caption “nlNJL” and labels for different values of the vector coupling η_V). Within this model approach we find that the vector coupling of the quark phase must be $\eta_V \geq 0.10$, otherwise the energy per baryon number E/A of the quark phase is lower than E/A in the hadron phase. On the other hand, very recent theoretical arguments [50] point that the vector channel interaction for quark matter might be small. Therefore, in this work we adopt $\eta_V = 0.10$ as the lowest value and $\eta_V = 0.20$ as the highest value.

C. Hadron-quark mixed phase under the Gibbs conditions

To take into account the finite-size effects, we impose the Gibbs conditions on the mixed phase [51], which require the pressure balance and the equality of the chemical potentials between two phases besides the thermal equilibrium. We employ the Wigner-Seitz approximation in which the whole space is divided into equivalent cells with given geometrical symmetry, specified by the dimensionality $d = 3$ (droplet or bubble), $d = 2$ (rod or tube), or $d = 1$ (slab). The structures of tube and bubble are opposite distributions of rod and droplet [52].

The quark and hadron phases are separated in each cell with volume V_W : a lump made of the quark phase with volume V_Q is embedded in the hadronic phase with volume V_H or vice versa. A sharp boundary is assumed between the two phases and the surface energy is taken into account in terms of a surface-tension parameter σ . Chiral quark model studies suggest values in the range $5 - 30 \text{ MeV fm}^{-2}$ [53–55], see also Ref. [56] where a range

of $145 - 165 \text{ MeV fm}^{-2}$ was found. In our calculations we use $\sigma = 10 \text{ MeV fm}^{-2}$ and $\sigma = 40 \text{ MeV fm}^{-2}$ and discuss the effects of its variation as in our previous studies with a simpler quark model [41].

We use the Thomas-Fermi approximation for the density profiles of hadrons and quarks. The Helmholtz free energy for each cell is then given as

$$E = \sum_{i=n,p} \int_{V_H} d^3\mathbf{r} \mathcal{E}_H[n_i(\mathbf{r})] + \sum_{q=u,d} \int_{V_Q} d^3\mathbf{r} \mathcal{E}_Q[n_q(\mathbf{r})] + E_e + E_C + E_S \quad (14)$$

with $i = n, p$, $q = u, d$, \mathcal{E}_H (\mathcal{E}_Q) is the free energy density for hadron (quark) matter, and $E_S = \sigma S$ the surface energy with S being the hadron-quark interface area. E_e is the free energy of the electron gas. For simplicity, muons are not included in this paper. The value of E_C is the Coulomb interaction energy calculated by,

$$E_C = \frac{e^2}{2} \int_{V_W} d^3\mathbf{r} d^3\mathbf{r}' \frac{n_{\text{ch}}(\mathbf{r}) n_{\text{ch}}(\mathbf{r}')}{|\mathbf{r} - \mathbf{r}'|}, \quad (15)$$

where the charge density is given by

$$en_{\text{ch}}(\mathbf{r}) = \sum_{i=n,p,e} Q_i n_i(\mathbf{r}) \quad (16)$$

in V_H and

$$en_{\text{ch}}(\mathbf{r}) = \sum_{q=u,d,e} Q_q n_q(\mathbf{r}) \quad (17)$$

in V_Q with Q_i (or Q_q) being the particle charge ($Q_e = -e < 0$ for the electron). Accordingly, the Coulomb potential $\phi(\mathbf{r})$ is defined as

$$\phi(\mathbf{r}) = - \int_{V_W} d^3\mathbf{r}' \frac{e^2 n_{\text{ch}}(\mathbf{r}')}{|\mathbf{r} - \mathbf{r}'|} + \phi_0, \quad (18)$$

where ϕ_0 is an arbitrary constant representing the gauge degree of freedom. We fix it by stipulating the condition, $\phi(R_W) = 0$, as in Refs. [38, 57, 58]. The Poisson equation then reads

$$\Delta\phi(\mathbf{r}) = 4\pi e^2 n_{\text{ch}}(\mathbf{r}). \quad (19)$$

Under the Gibbs conditions, we must consider chemical equilibrium at the hadron-quark interface as well as inside each phase

$$\begin{aligned} \mu_u + \mu_e &= \mu_d, \\ \mu_p + \mu_e &= \mu_n = \mu_u + 2\mu_d. \end{aligned} \quad (20)$$

For a given baryon number density

$$n_B = \frac{1}{V_W} \left[\sum_{i=n,p} \int_{V_H} d^3\mathbf{r} n_i(\mathbf{r}) + \sum_{q=u,d} \int_{V_Q} d^3\mathbf{r} \frac{n_q(\mathbf{r})}{3} \right], \quad (21)$$

Eqs. (19–20), together with the global charge neutrality condition,

$$\int_{V_W} d^3\mathbf{r} n_{\text{ch}}(\mathbf{r}) = 0,$$

obviously fulfill the Gibbs conditions.

D. Strangeness in compact stars?

The question arises whether it is customary to generalize the approach to the three-flavor case before attempting a comparison of results with compact star observables. We argue that our present restriction to the two-flavor case in the hadronic as well as in the quark matter phase in this work may be considered quite reliable. Starting with increasing density in hadronic matter one should expect the onset of hyperons to play a role for the compact star structure. It turns out, however, that the appearance of hyperons leads to a softening of neutron star matter which lowers considerably the maximum mass in contradiction with the observation of pulsars with masses of $\sim 2 M_\odot$ [4, 5]. This problem is known as the hyperon puzzle and its standard solution consists in circumventing the appearance of hyperons in neutron star matter by an early transition to quark matter [59]. For a recent discussion see [60, 61], and references therein. The occurrence of the strange quark flavor in quark matter, on the other hand is shown to be a sequential process within chiral quark models [62–64]. The reason for the sequential deconfinement in those models is that as a necessary condition the value of the quark chemical potential has to exceed that of the dynamically generated quark mass of a given flavor. As a result, the strange quark matter phases appear at higher densities than the two-flavor quark matter. Actually, as has been demonstrated before [65], the onset of strangeness in cold quark matter leads to a softening of matter which in particular for the three-flavor color superconducting (CFL) phase entails the instability of hybrid star configurations beyond that threshold. The onset of strange quark matter thus marks the end of the stable hybrid star configurations (maximum mass star). Following these arguments the structure of stable compact star configurations may well be devoid of strangeness in hadronic as well as in quark matter phases.

III. NUMERICAL RESULTS

A. Effects of the surface tension and the vector coupling on the EoS and on the finite-size structure

Using above relations, we study the hadron-quark mixed phase. The four panels of Fig. 2 show the resulting pressure of the hadron-quark mixed phase in comparison with that of the pure hadron and quark

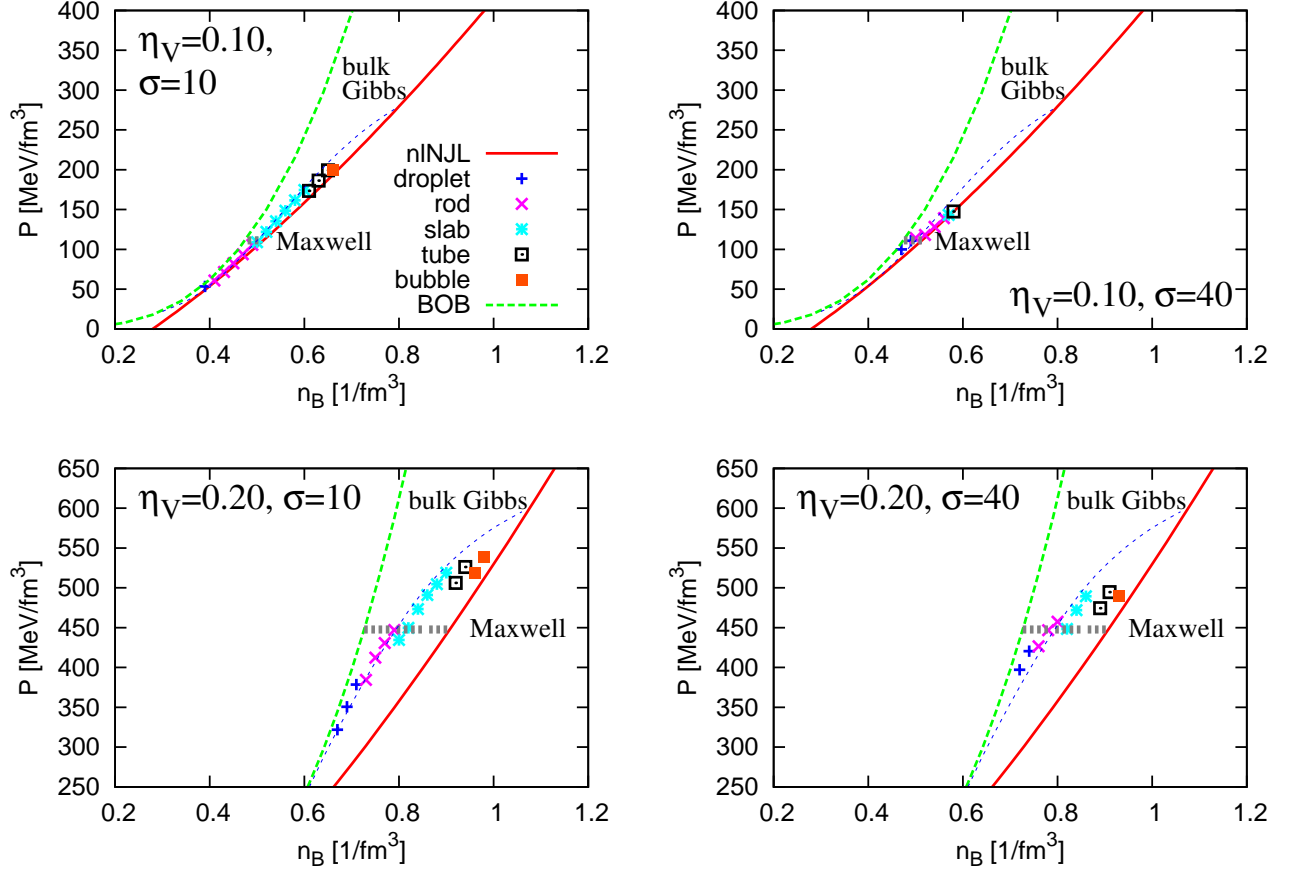


FIG. 2. (Color online) The EoS in terms of pressure p versus baryon density n_B for the pure hadronic BOB model (bold dashed line), the purely quark matter nNJL model (bold solid line) and three alternatives of the mixed phase construction: pasta phases of different structures (symbols) in comparison with the Maxwell construction (thick dotted line) and the bulk Gibbs construction (thin dashed line). The left (right) panels show results for the same surface tension $\sigma = 10$ (40) MeV fm^{-2} . The upper (lower) panels are for the same vector coupling $\eta_V = 0.10$ (0.20).

phases in the relevant range of baryon density for $\sigma = 10$ (40) MeV fm^{-2} on the left (right) panels and for $\eta_V = 0.10$ (0.20) on the upper (lower) panels. The bold dashed and solid lines indicate the pure hadron and quark phases, respectively, while the symbols indicate the mixed phase in its various geometric realizations obtained by the full calculation. The transitions between the different geometrical structures are, by construction, discontinuous and a more sophisticated approach would be required for a more realistic description of this feature. For comparison, the hadron-quark phase transition resulting from the Maxwell construction is shown by the thick, dotted gray line and the result of the bulk Gibbs construction by the thin, dashed blue line.

Compared with the case of weak surface tension ($\sigma = 10 \text{ MeV fm}^{-2}$), the mixed phase with strong surface tension ($\sigma = 40 \text{ MeV fm}^{-2}$) is restricted to a smaller density interval and the EoS gets closer to the one given by the Maxwell construction, even though we properly apply the Gibbs conditions. This reduction of the mixed phase region due to the charge screening and surface tension ef-

fects has already been demonstrated earlier for the case when a simple bag model is used for describing quark matter [38–41].

As shown in Fig. 1, the free energy per baryon E/A of the nNJL model becomes large for strong η_V . Hence we observe that the region of the mixed phase shifts to higher densities as the vector interaction is increased, see also Fig. 2. This behavior implies that the density region of the mixed phase becomes larger for stronger η_V .

Fig. 3 shows the free energy per baryon of the droplet structure for several values of surface tension at $\eta_V = 0.20$. The quark volume fraction $(R/R_W)^3$ is fixed to exclude the trivial R_W dependence. Here we use, for example, the optimal value of $(R/R_W)^3$ at $\sigma = 10 \text{ MeV fm}^{-2}$ for all curves. We normalize them by subtracting the free energy at infinite radius, $\Delta E/A = (E - E(R \rightarrow \infty))/A$, to show the R dependence clearly. Optimal sizes of R can be evaluated from the minimum energy of $\Delta E/A$ obeying the variational principle. The structure of the mixed phase is mechanically stable below $\sigma \sim 70 \text{ MeV fm}^{-2}$. For larger values of the surface tension the minimum dis-

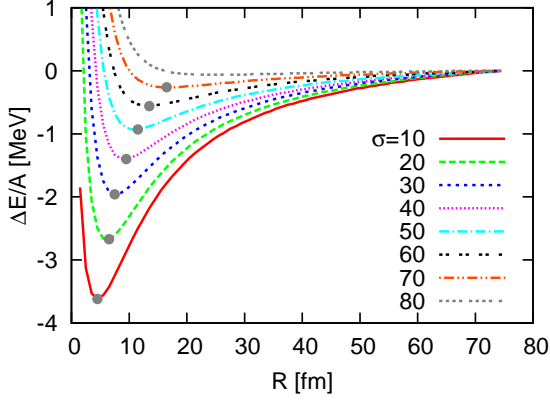


FIG. 3. (Color online) The dependence of the free energy per baryon on the droplet radius R at $n_B = 0.70 \text{ fm}^{-3}$ for different surface tensions. The quark volume fraction $(R/R_W)^3$ is fixed to the optimal value at $\sigma = 10 \text{ MeV fm}^{-2}$ for each curve. The free energy is normalized by its value at $R \rightarrow \infty$. Filled circles on each curve shows the minimum energy configuration.

appears so that the formation of finite-size structures is no longer favorable. The optimal value of the radius R is shifted to larger values as σ increases. This behavior is a signal of the mechanical instability resulting from the interplay between charge screening and surface tension effects. To elucidate this point more clearly, we discuss the contribution of E_S to E in Eq. (14). For a given quark volume fraction $\lambda = (R/R_W)^3$, the contribution of the surface energy on E/A is defined as

$$E_S/V_W \sim \lambda \frac{\sigma}{R}, \quad (22)$$

where V_W is the volume of the Wigner-Seitz cell. Hence, it is simply understood as $E_S/A \sim 1/R$. To reduce the total energy E , a large R is favored for a strong surface tension, which means that the effects of surface tension increase R . Similar results have been obtained in previous studies, although they adopted a simple bag model for the quark matter EoS [38–41].

When we treat the Coulomb potential and the charge densities in a self-consistent manner, we can see the charge screening effect. It gives rise to the Debye screening mass for the Coulomb interaction and induces the rearrangement of charge densities. In Fig. 4, the density profiles within a 3D cell (quark droplet) is shown for $n_B = 0.70 \text{ fm}^{-3}$ with weak (strong) surface tension, $\sigma = 10 \text{ MeV fm}^{-2}$ (40 MeV fm^{-2}) in the upper (lower) panel. We also fixed the vector interaction as $\eta_V = 0.20$, the same value as in Fig. 3. The electron density is continuous in this figure. But all the other densities are not since a sharp boundary is assumed between the two phases.

Although the values of the quark volume fraction $(R/R_W)^3$ and the cell sizes R_W are fixed in Fig. 3, their optimal values are also evaluated by the variational principle as shown in Fig. 4. The optimal cell sizes are

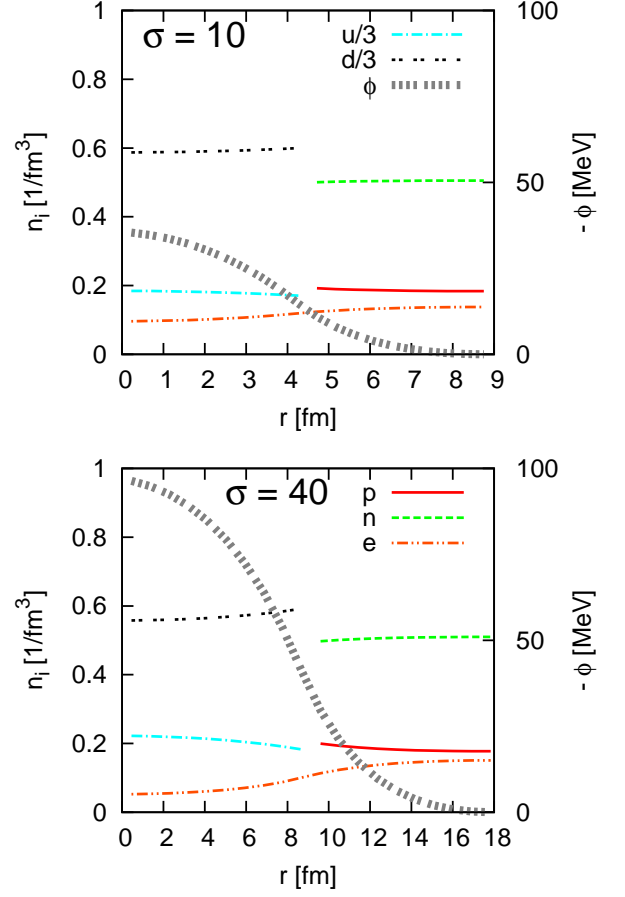


FIG. 4. (Color online) Density profiles and Coulomb potential ϕ for a 3D (quark droplet) when $n_B = 0.70 \text{ fm}^{-3}$ for $\sigma = 10 \text{ MeV fm}^{-2}$ (upper panel) and for $\sigma = 40 \text{ MeV fm}^{-2}$ (lower panel). The cell size is $R_W = 8.98 \text{ fm}$ (18.3 fm) with a droplet radius $R = 4.50 \text{ fm}$ (9.14 fm) for the surface tension $\sigma = 40 \text{ MeV fm}^{-2}$ (10 MeV fm^{-2}).

$R_W = 8.98 \text{ fm}$ for $\sigma = 10 \text{ MeV fm}^{-2}$, and $R_W = 18.3 \text{ fm}$ for $\sigma = 40 \text{ MeV fm}^{-2}$. The optimal droplet radii are $R = 4.50 \text{ fm}$ for $\sigma = 10 \text{ MeV fm}^{-2}$, and $R = 9.14 \text{ fm}$ for $\sigma = 40 \text{ MeV fm}^{-2}$. Clearly, for strong surface tension R_W is larger than for weak surface tension. The fraction $(R/R_W)^3$ depends only on the total baryon density. Hence, when the baryon density is conserved, R_W grows with R according to the increase in σ which is large for large σ as shown in Fig. 3. The effects of surface tension increase R_W mainly through the rearrangement of the charge densities. Since the properties of hadron matter inside the mixed phase are very different from those of pure hadron matter, hadron matter is positively charged and its partial density drops to zero in the mixed phase.

B. Effects on the particle fraction

Particle fractions of quark and hadron species are shown in Fig. 5. Left (right) panels show results for the

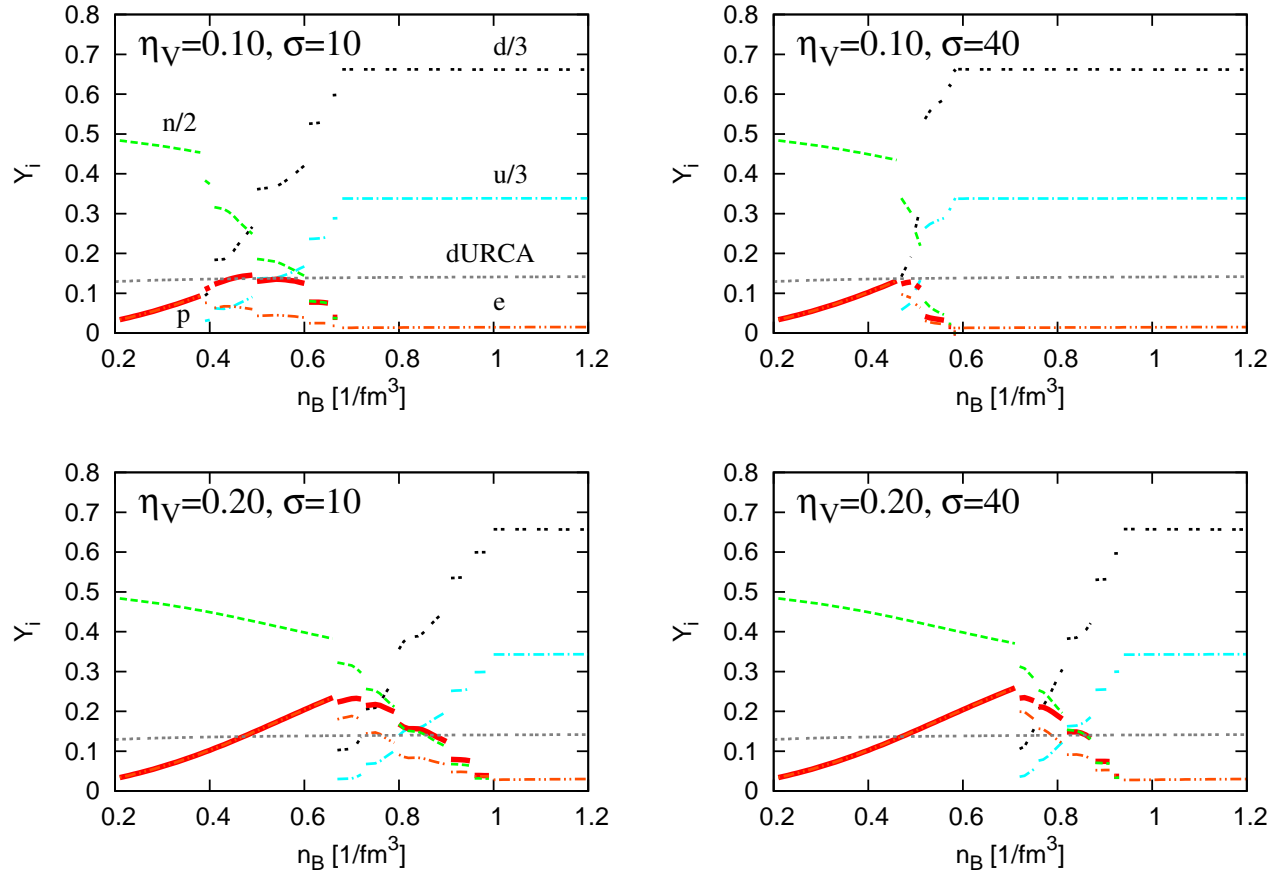


FIG. 5. (Color online) Left (right) panels show the particle fractions at weak (strong) surface tension $\sigma = 10 \text{ MeV fm}^{-2}$ (40 MeV fm^{-2}). The upper (lower) panels have weak (strong) vector couplings $\eta_V = 0.10$ (0.20).

weak (strong) surface tension with values $\sigma = 10 \text{ MeV fm}^{-2}$ (40 MeV fm^{-2}) for comparison. Upper (lower) panels are calculated with the vector coupling $\eta_V = 0.10$ (0.20). The discontinuities in the fractions are visible on all panels, since the mixed phases assume fixed geometrical symmetries.

We also show by the dotted, gray line the criterion for the onset of the dURCA process in $n-p-e$ matter, the threshold value $Y_p = 1/9$ for proton fraction. For proton fractions exceeding this value the dURCA process occurs which leads to rapid cooling of the neutron star in contradiction with observations, see e. g. Refs. [9, 66, 67]. One possible resolution to this problem is that the nuclear matter is superseded by quark matter as the density increases. See, e.g., the case of DBHF with Bonn-A in Ref. [65]. In the present case, with the vector channel strength $\eta_V = 0.10$ the thick, red curve on Fig. 5 shows the proton fraction below the dURCA value. For this picture to actually work, the dURCA process in quark matter needs to be suppressed, which can be accomplished by small quark pairing gaps that do not significantly influence the EoS [12]. Since at this stage our calculation of the quark phase does not take quark pairing into ac-

count our results are to be regarded as illustrative. If the vector coupling is stronger, $\eta_V = 0.20$, the onset of quark matter is delayed and the proton fraction exceeds the dURCA value.

C. Mass-radius and mass-central density sequences

In this section we discuss some implications of our results for the EoS on the maximum mass of neutron stars. We show the mass – radius ($M-R$) relations and the mass – central density ($M-n_{B,C}$) relations for isothermal hybrid stars in Fig. 6 and Fig. 7, respectively, obtained by solving the Tolman-Oppenheimer-Volkoff equations. Below the subnuclear density $n < 0.1 \text{ fm}^{-3}$, we use the BPS EoS [68]. In the figures 6 and 7, we also show the mass range $M = 2.01 \pm 0.04 M_\odot$ obtained from observational data for the pulsar PSR J0348+0432 by Antoniadis et. al [5]. All our models are clearly consistent with their result, and consequently also with the former high-mass constraint of $M = 1.97 \pm 0.04 M_\odot$ derived from observational data for PSR J1614-2230 by Demorest et al. [4].

We can see that the maximum mass M_{max} at the weak

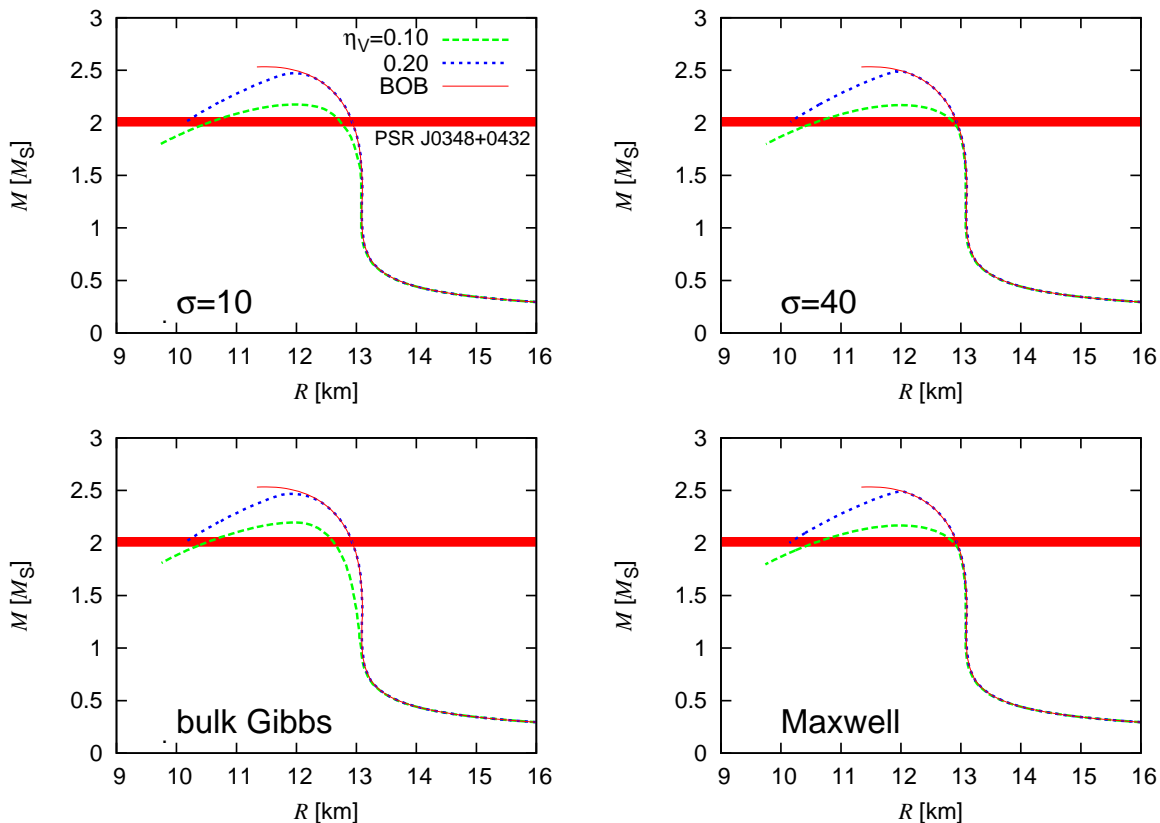


FIG. 6. (Color online) Mass-radius relations for the choice of EoS as shown in Fig. 2. The shaded area with shows the constraint of the mass measurement $M = 2.01 \pm 0.04 M_\odot$ obtained by Antoniadis et. al [5] from observational data for the pulsar PSR J0348+0432.

vector coupling $\eta_V = 0.10$ is slightly smaller than that at $\eta_V = 0.20$ for each surface tension. E.g., for $\sigma = 10 \text{ MeV fm}^{-2}$ we have $M_{\text{max}} = 2.17 M_\odot$ at $\eta_V = 0.10$ and $M_{\text{max}} = 2.49 M_\odot$ at $\eta_V = 0.20$. This result is easily understood from the fact that strong vector interactions increase the stiffness of the EoS. However, they are also responsible for the shift in the onset of the pure quark (or the mixed) phase as understood from the shift in the chemical potential. In addition, it turns out that the latter has a stronger impact on the stability of the star than the former. The trend is that for higher vector couplings the appearance of quarks makes the star unstable. For example, with $\eta_V = 0.20$ the hybrid star branch lies on the borderline of stability as seen from Figs. 6 and 7.

Finite-size effects have a strong influence on the composition of the star. It is interesting to consider the case of $\eta_V = 0.10$. By comparing the bulk Gibbs construction from Fig. 6 with Fig. 7 we deduce that the stable region of the hybrid star branch has only a mixed phase of quarks and nucleons since the central densities for which pure quark matter phases appear lie on the unstable branch. If we allow for finite-size effects, the same comparison leads to the conclusion that the hybrid branch contains stars with a mixed phase but also with a pure quark matter core. In particular, the cases of $\sigma = 10 \text{ MeV fm}^{-2}$

and $\sigma = 40 \text{ MeV fm}^{-2}$ as well as the limiting Maxwell construction have pure quark matter in the core of the heaviest stars. On the other hand, we find that finite-size effects have a small influence on the maximum mass. For the bulk Gibbs constructions (the extreme case of vanishing surface tension) the maximum mass is $2.19 M_\odot$ at $\eta_V = 0.10$, and with the EoS under the Maxwell construction (the extreme case of strong surface tension) it is $2.17 M_\odot$ at same η_V .

In Table I, we summarize the important quantities as discussed in this section categorized by the conditions of the phase transition and the strength of vector coupling. The conditions of the phase transition consist of the full calculations including the finite-size effects with the surface tension ($\sigma = 10, 40 \text{ MeV fm}^{-2}$), the bulk Gibbs and the Maxwell constructions. As described in Sec. II, we discussed as a weak vector coupling the value $\eta_V = 0.10$, and as a strong one $\eta_V = 0.20$. The columns “ n_1 ” and “ n_2 ” show the onset densities of the mixed and the pure quark phase, respectively. The maximum masses are shown by “ M_{max} ” in units of the solar mass M_\odot . The column “ n_{dU} ” shows the onset densities of the dURCA process. The last columns show the size of the pure quark matter r_2 , that of the mixed phase r_1 and the radius R for four different masses of the star: 1) the

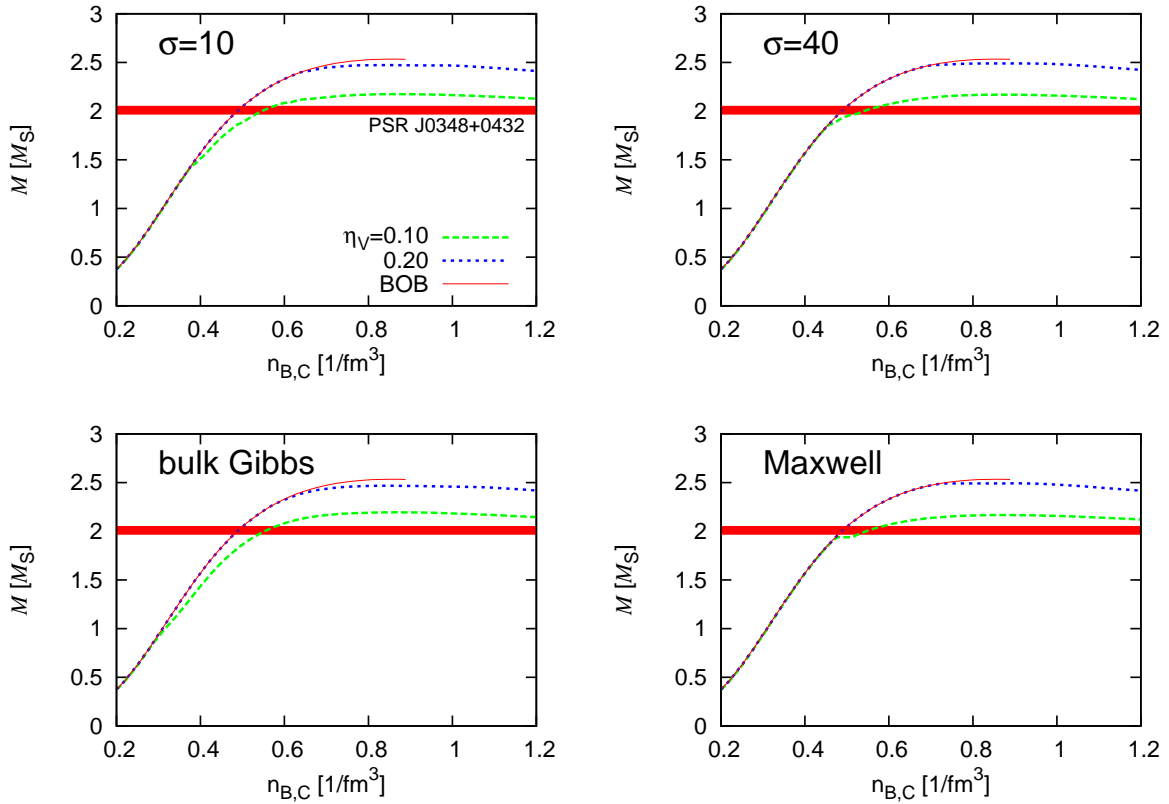


FIG. 7. (Color online) Same as Fig. 6, but for mass - central density sequences.

mass of a typical binary radio pulsar $M_{\text{BRP}} = 1.4 M_{\odot}$, 2) the presently largest of precisely measured masses $M_{\text{Antoniadis}} = 2.01 M_{\odot}$, 3) the mass at the onset of a pure quark matter core M_2 and 4) the maximum mass for the given case. Inspecting these results we make a few observations for the hybrid EoS presented in this work. At M_{BRP} , there is no pure quark matter core in compact stars. Even a mixed phase core does not occur, except for the extreme case of a bulk Gibbs construction for the weak vector coupling case, when it extends over a little more than half the radius. At the mass of the Antoniadis pulsar, $2.01 M_{\odot}$, for the weak vector coupling a quark matter core is expected in all cases (but only for the Maxwell construction this is pure quark matter) while for the stronger vector coupling there is none. When the mass is increased to that of the maximum stable configuration, then also in the case of a structured mixed phase a pure quark matter core is formed which extends over almost half the star's radius, followed by a mixed phase layer of thickness depending on the surface tension. From zero thickness for the Maxwell construction over 1.8 km for the larger surface tension to 3.9 km for the small surface tension. For vanishing surface tension in the bulk Gibbs construction case the whole quark matter core is in the mixed phase and extends up to 9.9 km, i.e. over more than 3/4 of the maximum mass star with a radius of 12.3 km.

IV. CONCLUSIONS AND DISCUSSION

We have studied the hadron-to-quark-matter phase transition with *finite-size effects* by imposing the Gibbs conditions on the phase equilibrium, and calculated the density profiles in a self-consistent manner. For the quark phase we used the covariant nonlocal NJL model, while the hadron phase was given by the BHF EoS with Bonn-B potential.

At strong surface tension, the EoS of the hadron-quark phase transition gets close to that given by the Maxwell construction. This is due to the mechanical instability of the geometrical structure induced by the surface tension. The pressure of the mixed phase shows a similar behavior to that of the bag model [38–41]. It appears that this behavior of the hadron-quark phase transition is universal. Since the EoS has many uncertainties, especially concerning quark matter we plan to study this behavior using other quark and hadron models such as [69]. Moreover, color superconductivity may also change our results [70, 71].

We have found that the models used here describe compact star sequences with maximum masses exceeding the present constraint of $\sim 2M_{\odot}$ as deduced from observations [4, 5]. For the low value of the vector coupling quarks appear at low densities, which might work in favor of suppressing the dURCA cooling channel in nuclear

TABLE I. A summary of our main results for hybrid star parameters with structures (pasta) in the mixed phase, categorized by the relative vector interaction strength η_V and the surface tension σ . For comparison, the extreme cases of the phase transition under the bulk Gibbs and the Maxwell constructions are shown which do not contain the finite-size effects, neither surface tension σ nor Coulomb interaction.

η_V	n_1	n_2	n_{dU}	M_{max}/M_\odot	At $M = M_{\text{BRP}}$			At $M = M_{\text{Anton}}$			At $M = M_2$			At $M = M_{\text{max}}$		
	[fm $^{-3}$]	[fm $^{-3}$]	[fm $^{-3}$]		r_2 [km]	r_1 [km]	R [km]	r_2	r_1	R	r_2	r_1	R	r_2	r_1	R
bulk Gibbs condition																
0.10	0.30	0.80	0.41	2.17	-	7.19	12.98	-	7.93	12.61	unstable			-	9.91	12.31
0.20	0.61	1.06	0.48	2.47	-	-	13.09	-	-	12.93	unstable			-	5.56	11.92
full calculation with pasta structures, $\sigma = 10 \text{ MeV fm}^{-2}$																
0.10	0.39	0.67	0.46	2.17	-	-	13.09	-	7.57	12.74	0	8.25	12.45	4.39	8.48	11.98
0.20	0.67	1.00	0.48	2.47	-	-	13.09	-	-	12.93	unstable			-	4.25	11.96
full calculation with pasta structures, $\sigma = 40 \text{ MeV fm}^{-2}$																
0.10	0.47	0.58	-	2.17	-	-	13.09	-	4.32	12.87	0	5.78	12.65	5.41	7.20	11.98
0.20	0.70	0.94	0.48	2.49	-	-	13.09	-	-	12.93	unstable			-	3.01	11.96
Maxwell construction																
0.10	0.48	0.51	-	2.17	-	-	13.09	3.33	3.33	12.88	0	0	12.96	6.76	6.76	11.84
0.20	0.73	0.91	0.48	2.49	-	-	13.09	-	-	12.93	0	0	12.03	0	0	12.03

matter by the early onset of quark matter. If we conjecture that future observations would find quark matter in neutron stars our results would indicate that vector interactions in the quark phase are small, unlike the ones in nuclear matter.

Since the phase transition to quark matter leads to a softening of the EoS, this is usually associated with the reduction in the maximum mass. The fact that the nuclear EoS employed in this work gives a neutron star surpassing $2M_\odot$ therefore works in favour of obtaining a sufficiently heavy hybrid star to exceeding $2M_\odot$ as well. However, we should keep in mind that this statement depends on the relative stiffness of the nuclear and the quark EoS at the highest densities reached in the core. There are notable exceptions in the literature, see e. g. [41, 59–61, 72] where one finds an opposite scenario so that the maximum mass of the hybrid star is actually larger than the maximum mass of the pure nuclear star.

In the context of the microscopically founded EoS model presented in this paper with the BHF approach to the hadronic phase and the nonlocal chiral quark model for the deconfined phase, the nonstrange hybrid star scenario appears as the most conservative one. Scenarios including strangeness in the hadronic and/or quark matter phase may require additional stiffening effects, that are beginning to be explored [73], in order to meet the $2M_\odot$ mass constraint. We shall return to such scenarios in subsequent work.

ACKNOWLEDGMENTS

We are grateful to H. J. Schulze, G. F. Burgio, M. Baldo for their warm hospitality and fruitful discussions. This work was supported by JSPS KAKENHI Grant Numbers 25105510, 23540325, 24105008, and by the Polish National Science Centre (NCN) under grant number UMO-2011/02/A/ST2/00306. S. B. is supported

by the University of Zagreb under Contract No. 202348 and by the MIAU project of the Croatian Science Foundation. D. B. acknowledges acknowledges Grant No. 1009/S/IFT/14 529 from the Polish Ministry of Science and Higher Education 530 (MNiSW).

-
- [1] A. W. Steiner, J. M. Lattimer and E. F. Brown, *Astrophys. J.* **722**, 33 (2010).
- [2] A. W. Steiner, J. M. Lattimer and E. F. Brown, *Astrophys. J.* **765**, L5 (2013).
- [3] D. B. Blaschke, H. A. Grigorian, D. E. Alvarez-Castillo and A. S. Ayriyan, *J. Phys. Conf. Ser.* **496**, 012002 (2014).
- [4] P. Demorest, T. Pennucci, S. Ransom, M. Roberts and J. Hessels, *Nature* **467**, 1081 (2010).
- [5] J. Antoniadis, P. C. C. Freire, N. Wex, T. M. Tauris, R. S. Lynch, M. H. van Kerkwijk, M. Kramer and C. Bassa *et al.*, *Science* **340**, 6131 (2013).
- [6] S. Bogdanov, *Astrophys. J.* **762** (2013) 96.
- [7] P. Podsiadlowski, *et al.*, *Mon. Not. Roy. Astron. Soc.* **361**, 1243 (2005).
- [8] F. S. Kitaura, H.-Th. Janka, W. Hillebrandt, *Astron. & Astrophys.* **450**, 345 (2006).
- [9] D. Page, M. Prakash, J. M. Lattimer and A. Steiner, *Phys. Rev. Lett.* **85**, 2048 (2000).
- [10] D. Blaschke, T. Klähn and D. N. Voskresensky, *Astrophys. J.* **533**, 406 (2000).
- [11] D. Blaschke, H. Grigorian and D. N. Voskresensky, *Astron. Astrophys.* **368**, 561 (2001).
- [12] H. Grigorian, D. Blaschke and D. Voskresensky, *Phys. Rev. C* **71**, 045801 (2005).
- [13] L. -M. Lin, K. S. Cheng, M. -C. Chu and W. -M. Suen, *Astrophys. J.* **639**, 382 (2006).
- [14] N. Yasutake, K. Kotake, M. -a. Hashimoto and S. Yamada, *Phys. Rev. D* **75**, 084012 (2007).
- [15] E. B. Abdikamalov, H. Dimmelmeier, L. Rezzolla and J. C. Miller, *Mon. Not. Roy. Astron. Soc.* **394**, 52 (2009).
- [16] T. Hatsuda, *Mod. Phys. Lett. A* **2**, 805 (1987).
- [17] K. 'i. Nakazato, K. Sumiyoshi and S. Yamada, *Phys. Rev. D* **77**, 103006 (2008).
- [18] I. Sagert, T. Fischer, M. Hempel, G. Pagliara, J. Schaffner-Bielich, A. Mezzacappa, F. -K. Thielemann and M. Liebendorfer, *Phys. Rev. Lett.* **102**, 081101 (2009).
- [19] G. F. Burgio, H. J. Schulze and F. Weber, *Astron. Astrophys.* **408**, 675 (2003).
- [20] D. N. Aguilera, D. Blaschke and H. Grigorian, *Astron. Astrophys.* **416**, 991 (2004).
- [21] N. Yasutake, M. -a. Hashimoto and Y. Eriguchi, *Prog. Theor. Phys.* **113**, 953 (2005).
- [22] J. L. Zdunik, M. Bejger, P. Haensel and E. Gourgoulhon, *Astron. Astrophys.* **465**, 533 (2007).
- [23] N. Ishii, S. Aoki and T. Hatsuda, *Phys. Rev. Lett.* **99**, 022001 (2007), and their series of papers.
- [24] A. Walker-Loud, *PoS LATTICE* **2013**, 013 (2013).
- [25] M. Baldo, *Nuclear Methods and the Nuclear Equation of State*, World Scientific, Singapore (1999).
- [26] A. Akmal, V. R. Pandharipande and D. G. Ravenhall, *Phys. Rev. C* **58**, 1804 (1998).
- [27] M. Takano, H. Togashi and H. Kanzawa, *Prog. Theor. Phys. Suppl.* **186**, 63 (2010).
- [28] R. Brockmann and R. Machleidt, *Phys. Rev. C* **42**, 1965 (1990).
- [29] E. N. E. van Dalen, C. Fuchs and A. Faessler, *Nucl. Phys. A* **744**, 227 (2004).
- [30] G. A. Contrera, M. Orsaria and N. N. Scoccola, *Phys. Rev. D* **82**, 054026 (2010).
- [31] S. Benic, D. Blaschke, G. A. Contrera and D. Horvatic, *Phys. Rev. D* **89**, 016007 (2014).
- [32] D. E. Alvarez-Castillo, S. Benic, D. Blaschke and R. Lastowiecki, *Acta Phys. Polon. Supp.* **7**, no. 1, 203 (2014).
- [33] M. B. Parappilly, P. O. Bowman, U. M. Heller, D. B. Leinweber, A. G. Williams and J. BZhang, *Phys. Rev. D* **73**, 054504 (2006).
- [34] W. Kamleh, P. O. Bowman, D. B. Leinweber, A. G. Williams and J. Zhang, *Phys. Rev. D* **76**, 094501 (2007).
- [35] M. S. Bhagwat, M. A. Pichowsky, C. D. Roberts and P. C. Tandy, *Phys. Rev. C* **68**, 015203 (2003).
- [36] C. S. Fischer and J. A. Mueller, *Phys. Rev. D* **80**, 074029 (2009).
- [37] C. D. Roberts, arXiv:1203.5341 [nucl-th].
- [38] D. N. Voskresensky, M. Yasuhira and T. Tatsumi, *Phys. Lett. B* **541**, 93 (2002).
- [39] D. N. Voskresensky, M. Yasuhira and T. Tatsumi, *Nucl. Phys. A* **723**, 291 (2003).
- [40] T. Endo, T. Maruyama, S. Chiba and T. Tatsumi, *Prog. Theor. Phys.* **115**, 337 (2006).
- [41] T. Maruyama, S. Chiba, H. -J. Schulze and T. Tatsumi, *Phys. Rev. D* **76**, 123015 (2007).
- [42] D. B. Blaschke, D. Gomez Dumm, A. G. Grunfeld, T. Klähn and N. N. Scoccola, *Phys. Rev. C* **75**, 065804 (2007).
- [43] M. Orsaria, H. Rodrigues, F. Weber and G. A. Contrera, *Phys. Rev. D* **87**, 023001 (2013).
- [44] S. Noguera and N. N. Scoccola, *Phys. Rev. D* **78**, 114002 (2008).
- [45] H. J. Schulze, A. Lejeune, J. Cugnon, M. Baldo and U. Lombardo, *Phys. Lett. B* **355**, 21 (1995).
- [46] M. Baldo, G. F. Burgio and H. J. Schulze, *Phys. Rev. C* **58**, 3688 (1998).
- [47] I. Vidana, A. Polls, A. Ramos, M. Hjorth-Jensen and V. G. J. Stoks, *Phys. Rev. C* **61**, 025802 (2000).
- [48] R. Machleidt, K. Holinde and C. Elster, *Phys. Rept.* **149**, 1 (1987).
- [49] B. S. Pudliner, V. R. Pandharipande, J. Carlson, S. C. Pieper and R. B. Wiringa, *Phys. Rev. C* **56**, 1720 (1997).
- [50] J. Steinheimer and S. Schramm, arXiv:1401.4051 [nucl-th].
- [51] H. Heiselberg, C. J. Pethick and E. F. Staubo, *Phys. Rev. Lett.* **70**, 1355 (1993).
- [52] N. Yasutake, T. Noda, H. Sotani, T. Maruyama and T. Tatsumi, in "Recent Advances in Quarks Research", H. Fujikage, K. Hyobanshi (Eds.) Nova Science Publishers, Ch. 4, pp. 63 (2013), [arXiv:1208.0427].
- [53] L. F. Palhares and E. S. Fraga, *Phys. Rev. D* **82**, 125018 (2010).
- [54] M. B. Pinto, V. Koch and J. Randrup, *Phys. Rev. C* **86**, 025203 (2012).
- [55] B. W. Mintz, R. Stiele, R. O. Ramos and J. Schaffner-Bielich, *Phys. Rev. D* **87**, 036004 (2013).
- [56] G. Lugones, A. G. Grunfeld and M. Al Ajmi, *Phys. Rev. C* **88**, 045803 (2013).
- [57] T. Tatsumi, M. Yasuhira and D. N. Voskresensky, *Nucl. Phys. A* **718**, 359 (2003).
- [58] T. Maruyama, T. Tatsumi, D. N. Voskresensky, T. Tanigawa and S. Chiba, *Phys. Rev. C* **72**, 015802 (2005).

- [59] M. Baldo, G. F. Burgio and H. J. Schulze 2003, in “Superdense QCD Matter and Compact Stars”, Proceedings of the NATO Advanced Research Workshop, Springer, Nato Science Series II, D. Blaschke, D. Sedrakian (Eds.) Vol. 197, pp. 113 (2006), [arXiv:0312446].
- [60] R. Lastowiecki, D. Blaschke, H. Grigorian and S. Typel, *Acta Phys. Polon. Supp.* **5**, 535 (2012)
- [61] J. L. Zdunik and P. Haensel, *Astron. Astrophys.* **551**, A61 (2013)
- [62] C. Gocke, D. Blaschke, A. Khalatyan and H. Grigorian, [hep-ph/0104183].
- [63] D. Blaschke, F. Sandin, T. Klähn and J. Berdermann, *Phys. Rev. C* **80**, 065807 (2009)
- [64] D. Blaschke, T. Klähn, R. Lastowiecki and F. Sandin, *J. Phys. G* **37**, 094063 (2010).
- [65] T. Klähn, D. Blaschke, F. Sandin, C. Fuchs, A. Faessler, H. Grigorian, G. Röpke and J. Trümper, *Phys. Lett. B* **654**, 170 (2007).
- [66] D. Blaschke and H. Grigorian, *Prog. Part. Nucl. Phys.* **59**, 139 (2007).
- [67] S. Popov, H. Grigorian and D. Blaschke, *Phys. Rev. C* **74**, 025803 (2006).
- [68] G. Baym, C. Pethick and P. Sutherland, *Astrophys. J.* **170**, 299 (1971).
- [69] H. Chen, G. F. Burgio, H. -J. Schulze and N. Yasutake, *Astron. and Astrophys.* 551, A **13** (2013).
- [70] G. Pagliara and J. Schaffner-Bielich, *Phys. Rev. D* **77**, 063004 (2008).
- [71] T. Klähn, D. B. Blaschke and R. Lastowiecki, *Phys. Rev. D* **88**, 085001 (2013).
- [72] M. G. Alford, S. Han and M. Prakash, *Phys. Rev. D* **88**, no. 8, 083013 (2013)
- [73] S. Benic, arXiv:1401.5380.